Deep-Sea Research II 58 (2011) 1485–1496

Contents lists available at ScienceDirect

Deep-Sea Research II

journal homepage: www.elsevier.com/locate/dsr2

Carbon export associated with free-drifting icebergs in the Southern Ocean

K.L. Smith Jr.[1,*], A.D. Sherman[1], T.J. Shaw[2], A.E. Murray[3], M. Vernet[4], A.O. Cefarelli[5]

[1] Monterey Bay Aquarium Research Institute, 7700 Sandholdt Rd, Moss Landing, CA 95039, USA
[2] Department of Chemistry and Biochemistry, University of South Carolina, Columbia, SC 29208, USA
[3] Desert Research Institute, 2215 Raggio Parkway, Reno, NV 89512, USA
[4] Scripps Institution of Oceanography, 8615 Discovery Way, La Jolla, CA 92037, USA
[5] Departamento Científico Ficología, Facultad de Ciencias Naturales y Museo, Universidad Nacional de La Plata, Paseo del Bosque s/n, 1900 La Plata, Argentina

ARTICLE INFO

Article history:
Received 12 November 2010
Accepted 12 November 2010
Available online 21 December 2010

Keywords:
Carbon export
Icebergs
Lagrangian sediment traps
Particulate organic carbon flux
Pelagic community
Weddell Sea

ABSTRACT

Enrichment of the pelagic ecosystem associated with the proliferation of free-drifting icebergs prompts questions about increased productivity and the export flux of organic carbon to the deep ocean with continued climate warming. Lagrangian Sediment Traps (LST) were deployed autonomously beneath a large tabular, free-drifting iceberg (C-18a) in the NW Weddell Sea during March and April 2009 to collect sinking particles at a depth of 600 m. Three LST deployments associated with C-18a, within a 30-km radius, collected sinking diatom frustules, dominated by *Corethron pennatum* and *Fragilariopsis nana*, euphausiid fragments, crustacean and fish fecal material, detrital aggregates and mineral grains. One LST deployment at a "control" site 74 km away in open water devoid of icebergs collected diatom frustules, euphausiid molts, crustacean fecal material and detrital aggregates. Phytoplankton abundance, microbial abundance and biomass were significantly higher in the LST samples than in open-water collections at 500 m depth. The mean mass flux and organic carbon flux associated with iceberg C-18a were twice as high, 124 mg m^{-2} d^{-1} and 5.6 mg C_{org} m^{-2} d^{-1}, respectively, than at the control site. A similar trend was observed in $C_{org}/^{234}Th$ activity, being highest near C-18a and lowest at the control site. Extrapolation of the area of enrichment to 30 km radius around C-18a, 2826 km^2, produces an estimated mass flux of 350 tons d^{-1} and carbon flux of 15.8 tons C_{org} d^{-1}. Five similar sized icebergs to C-18a were identified in satellite images in a surrounding 47,636 km^2 area at the same time of sampling. Assuming a 30-km radius as the area of influence around each of these five icebergs, 46% of the total area would be enhanced with an export flux at 600 m of 122.4 tons C_{org} d^{-1}. The large numbers of smaller icebergs identified visually in this area would only increase this area of influence. Icebergs serve as areas of local enrichment and with increased proliferation, must be considered in the cycling of carbon in the Southern Ocean.

1. Introduction

How important is the Southern Ocean in the global carbon cycle with increasing CO_2 levels and global warming? The importance of the draw-down of atmospheric carbon in the Southern Ocean and its ultimate sequestration are topics of considerable debate (Hoppema, 2004; Le Quere et al., 2007). The high-nutrient/low-chlorophyll (HNLC) waters of the Southern Ocean when artificially fertilized with iron, yield increased rates of primary production, thus increasing the amount of CO_2 drawn down into phytoplankton biomass. However, there are conflicting reports as to how much of this carbon is ultimately exported from the surface waters and reaches the deep sea. Artificial, mesoscale iron-enrichment experiments have enhanced diatom biomass (Boyd et al., 2000; Coale et al., 2004) and thus increased the drawdown of CO_2. However, over the short time periods of these experiments, the export of fixed carbon and its deep-sea sequestration are equivocal (Boyd, 2004; Buesseler et al., 2004; Lam and Bishop, 2007). Natural iron fertilization experiments, where upwelled iron provides the enrichment source, have provided good evidence that the increased phytoplankton biomass production is exported to deeper depths in the Southern Ocean at significantly higher rates than adjacent areas not fertilized by iron (Pollard et al., 2009; Blain et al., 2007). It is argued that under natural conditions, there is ample time for food chain transfer of this carbon through zooplankton grazing and fecal material export into the deep ocean (e.g., Ebersbach and Trull, 2008).

Other sources of iron include aerosols and glacially derived icebergs. Aerosol iron can enhance primary production in the Southern Ocean, especially in areas downwind of dry continental areas (Cassar et al., 2007). However, given the slow dissolution of iron in seawater, such dust mediated enhancement of primary

* Corresponding author. Tel.: +1 831 775 1710.
E-mail address: ksmith@mbari.org (K.L. Smith Jr.).

0967-0645/$ - see front matter © 2010 Elsevier Ltd. All rights reserved.
doi:10.1016/j.dsr2.2010.11.027

production is considered rare (Boyd et al., 2009). Recent evidence suggests that free-drifting icebergs in the Southern Ocean contain significant concentrations of terrigenous material and are areas of enriched phytoplankton and zooplankton production (Smith et al., 2007). This terrigenous material, of glacial and aeolian origin, contributes significant concentrations of iron into the surrounding water (Lin et al., 2011), thus forming a natural enrichment experiment with a pelagic foodweb capable of processing photosynthetically derived organic carbon. Gen the increased number of icebergs in the Southern Ocean (Ballantyne, 2002), we hypothesized that there should be substantial carbon export and sequestration associated with these enrichment sites compared to open water some distance away.

2. Methods

To measure the flux of carbon associated with an iceberg, we developed an autonomous instrument that would collect sinking particulate matter while floating below the iceberg at a predetermined depth (Sherman et al., 2011). The Lagrangian Sediment Trap (LST) was designed around an existing neutrally buoyant SOLO float (Sounding Oceanographic Lagrangian Observer; Davis et al., 2001) and then adding four sampling funnels and opening-closing cups to collect sinking particles at a pre-determined depth of $\sim$600 m. Each collection funnel had a mouth opening of 0.08 m^2 for a total collection surface area of 0.32 m^2. The LST was deployed autonomously from the RVIB Nathaniel B. Palmer in March and April 2009 to sample at a depth of 600 m under and in the vicinity of a large tabular iceberg, C-18a, in the northwestern Weddell Sea.

Prior to each deployment, each LST sample cup (125 ml) was filled with filtered surface seawater. No preservative was added to the LST sample cups since the deployment periods were less than four days (2.5 to 3.8 d) with assumed slow degradation at $<$ 0.5 °C. The descent of the LST with a disposable weight of 7 kg was sufficient to attain a sinking speed of 8 m s^{-1}, reaching 600 m in $\sim$62 s. Upon release of the descent weight at $\sim$600 m depth, the sample cups sprung open for collection of particles. At the end of the collection period, the sample cups were then closed with a burn-wire release just before the LST ascended to the surface after releasing the ballast weight. The closure mechanism failed to rotate completely on three deployments (Stas. 95,96,142) and thus the cups were partially open at the base of the collection funnels contributing possible contaminants or winnowing the collected material during the $\sim$96-minute ascents to the surface from 600 m. Once the LST was visually located on the surface, a small boat was deployed and the sample cups removed while the instrument was still vertically oriented in the water to prevent possible loss of samples. The period from surfacing to sample recovery was $<$30 minutes. The capped sample cups and LST were returned to the ship and the samples kept on ice until further processing.

One sample cup from each deployment was subsampled for microscopy and bacterioplankton analyses of the freshly collected material. A low magnification stereomicroscope (6.5X to 50X) was used to examine and photograph the larger particulate matter in etched-glass grid petri dishes. The particulate matter in a small 5-ml subsample was examined and photographed with finer resolution using a high-magnification compound microscope. Samples in water mounts were analyzed at either 100, 200 or 400X in bright or phase contrast with a Zeiss Axioscop 50. Photographs were taken with a digital camera SPOT RT slider. Small subsamples were preserved in formalin for further microscopic analysis ashore. Mineral phases in these samples were determined by microscopic examination but sample size limitations precluded separate digestions for mineral content. In addition, a 50-ml subsample was taken for bacterioplankton analyses. The remaining three samples were filtered onto quartz membrane filters, conspicuous swimmers removed, and frozen at -80 °C. In the laboratory the filters were dried at 60 °C for 24 hours and then weighed to determine total mass. Half of each filter was then analyzed for total carbon and nitrogen using a Control Equipment Corporation Elemental Analyzer (Model 240XA). The other half of each filter was moistened with 10% v/v HCL, held in a closed container for 24 hours and then placed in a 60 °C drying oven for an additional 24 hours. The loss of mass measured after HCl treatment was considered inorganic carbon. The dried samples were then analyzed for carbon, and nitrogen using the elemental analyzer above with the resulting carbon concentrations assumed to be organic.

Samples from a single LST cup from each deployment were mixed then subsampled for cell counts and leucine incorporation rate determination. The leucine incorporation method (Kirchman et al., 1986) was adapted to the microcentrifugation method (Smith and Azam, 1992). Triplicate 1.5 ml subsamples and a single TCA-killed control sample were prepared for each LST sample, 20 nM final concentration 3 H-leucine was added, and the samples incubated at 0 °C in water baths for 2-3 hours. Following incubations, the samples were stopped by addition of TCA (5% final concentration), and following centrifugation and washes with 5% TCA, the pellets were dried with 80% ethanol. Due to the low volumes available from the LST sample, 1–1.5 ml were prepared for microscopy. Samples were vortexed, and enumeration of DAPI-stained bacterial cells following fixation in formalin using standard methods (Porter and Feig, 1980).

One sample cup from each LST deployment was filtered on a Quartz Membrane Filter (QMF) and dried for determination of the organic carbon to ^{234}Th activity ratio as a proxy for organic carbon export (see Shaw et al., 2011a). The ^{234}Th activity was measured on a shipboard Riso Beta counter with backgrounds determined later in the laboratory. CHN analyses were conducted as described above after background counts were complete.

3. Results

Four deployments of the LSTs were achieved, sampling beneath and around iceberg C-18a and then at a "control" station $\sim$74 km distance. These deployments were conducted in the NW Weddell Sea from 18 March through 7 April 2009 while C-18a was free-drifting between 61° and 62° S and between 49° and 52° W (Fig. 1). The overall water depth during the four deployments ranged from 2918 to 3277 m over the Powell Basin.

Iceberg C-18a was formed in the Ross Sea during a calving event in 2003. This tabular iceberg then drifted counterclockwise around the Antarctic continent before reaching the NW Weddell Sea and being entrained in a northerly flow dubbed "Iceberg Alley" (Smith, 2011; Stuart and Long, 2011). The estimated dimensions of C-18a were 35 km long and 6 km wide with an aerial height of 28 m at the time of sampling (Helly et al., 2011). Although the iceberg draft was not accurately measured, it was estimated from ROV dives to extend $\sim$200 m below the surface (Sherlock et al., 2011) which is consistent with other Antarctic iceberg studies (Dowdeswell and Bamber, 2007). Iceberg C-18a rotated as much as 60° while maintaining a general north-south orientation in a northeasterly direction at 0.2 to 0.4 km hr^{-1} (Helly et al., 2011).

3.1. Description of particulate matter:

On the first deployment (Sta. 43), the LST was launched in front of C-18a, as it drifted over the instrument which was

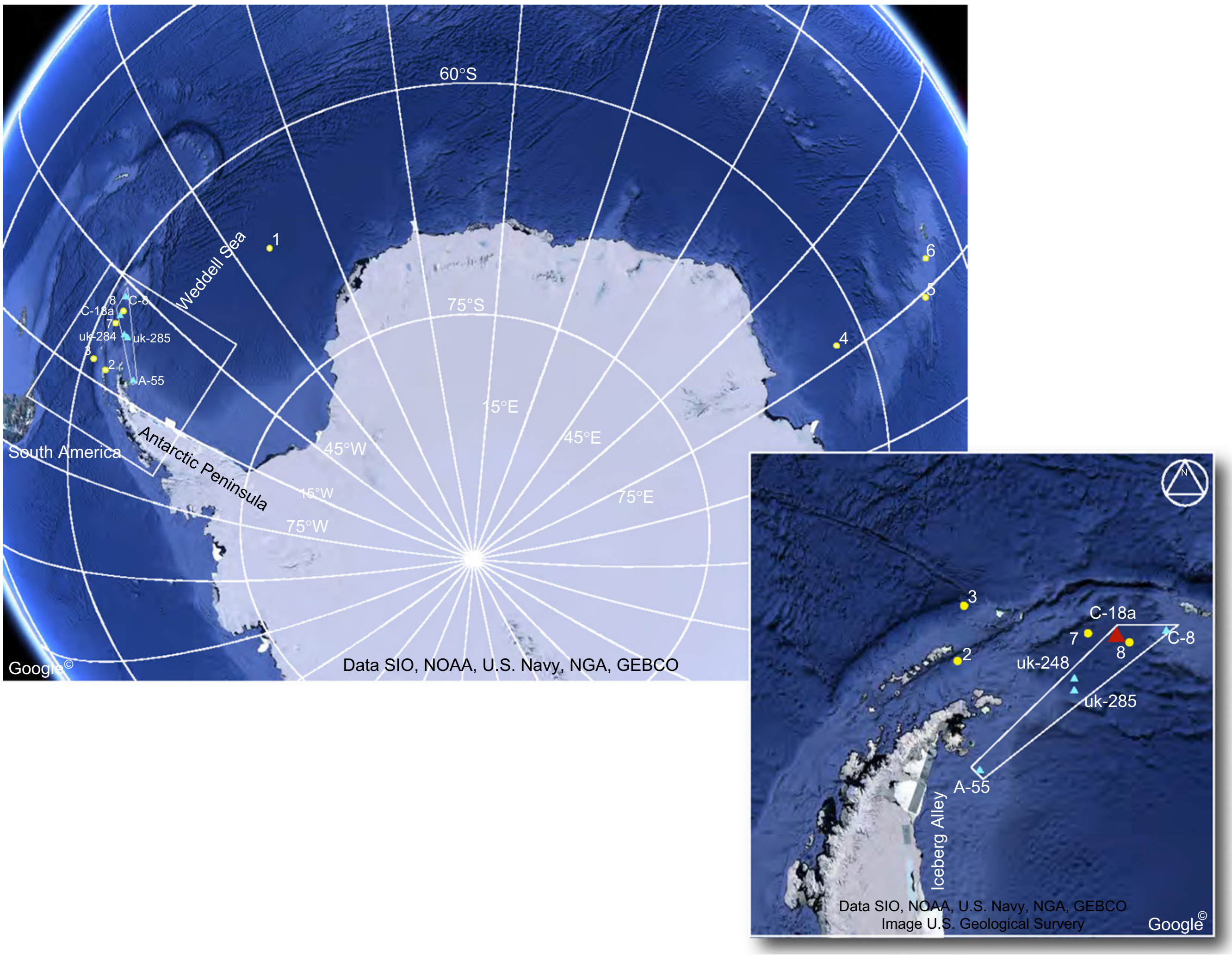

Fig. 1. Chart showing the Antarctic Peninsula, Weddell Sea and the Southern Ocean extending to the Southern Indian Ocean. The study site around iceberg C-18a (red triangle) including the satellite survey area containing five icebergs (C-8, C-18a, uk-284, uk-285 and A-55). The sites of six sediment trap deployments made at comparable depth and time of year ranging from the NW Weddell Sea and Bransfield Strait to the Southern Indian Ocean (#1 – N. Weddell Sea, #2 – Bransfield Strait, #3 Drake Passage, #4 – Southern Indian Ocean, #5 – Kerguelen Plateau, and #6 – Crozet Plateau (see Table 3 for site details).

neutrally buoyant at ~600 m depth. The LST was then recovered 2.9 days later at a distance of 7.8 km north of the deployment site (Fig. 2A). The particulate material in the four collection cups consisted of eight taxa of diatoms (Table 1), which appeared dominated by *Corethron pennatum*, with frustules containing cellular material in varying stages of degradation (Fig. 3A). However, under more stable microscope conditions ashore, *Fragilariopsis nana*, a small diatom 2.4–15.5 μm in length was the most numerically abundant species. The diatom taxa, combined with silicoflagellates and radiolarians formed detrital aggregates (Fig. 3B). Fragments of euphausiids (Fig. 3C) and their cylindrical string fecal pellets (Fig. 3D) were abundant as well as fecal material from small crustaceans and fish (Table 1).

During each LST deployment, a series of transmissometer casts were taken in the vicinity to estimate particle density from light transmission as part of routine CTD casts (Smith, 2011). Fourteen transmission profiles during the first deployment showed percent transmissivity between 93.5 and 95.5 in the surface waters, rapidly increasing to >98% below 100 m depth (Fig. 4). At 600 m depth the percent light transmission was consistently above 98%, indicating low suspended particle density in water with a salinity of 34.66 psu and temperature of 0.46 °C.

The second deployment (Sta. 95) of the LST was again set so that iceberg C-18a drifted over the instrument. The 3.8-day collection period of sinking particulate matter on this deployment resulted in the LST drifting 32.4 km southeast before recovery (Fig. 2B). Over this collection period at ~600 m depth, diatoms were prevalent and again numerically dominated by *F. nana* and *C. pennatum* of the six taxa present (Table 1). There was considerable diversity in zooplankton and micronekton fecal material with euphausiid string and ovoid pellets (Fig. 3F) being most numerous. Salp fecal material (Fig. 3G, H) was evident as well as the more amorphous fecal fluff. A euphausiid molt (Fig. 3E) and exoskeleton fragments (Fig. 3G) were conspicuous components.

The third deployment (Sta. 96) of the LST drifted under C-18a and continued for a total distance of 40.6 km at 600 m depth over the course of 3.5 days (Fig. 2C). The collected particulate matter was similar in composition to that in the previous deployments (Table 1). There was a greater diversity of diatom taxa totaling 11, dominated by *F. nana* and *C. pennatum*, but with many broken frustules amongst the phytodetrital aggregations (Fig. 3I). Fecal material was dominated by euphausiid string pellets (Fig. 3 K, L) and ovoid crustacean pellets (Fig. 3J). Radiolarians were also numerous, serving as nuclei for agglutinating phytodetritus and

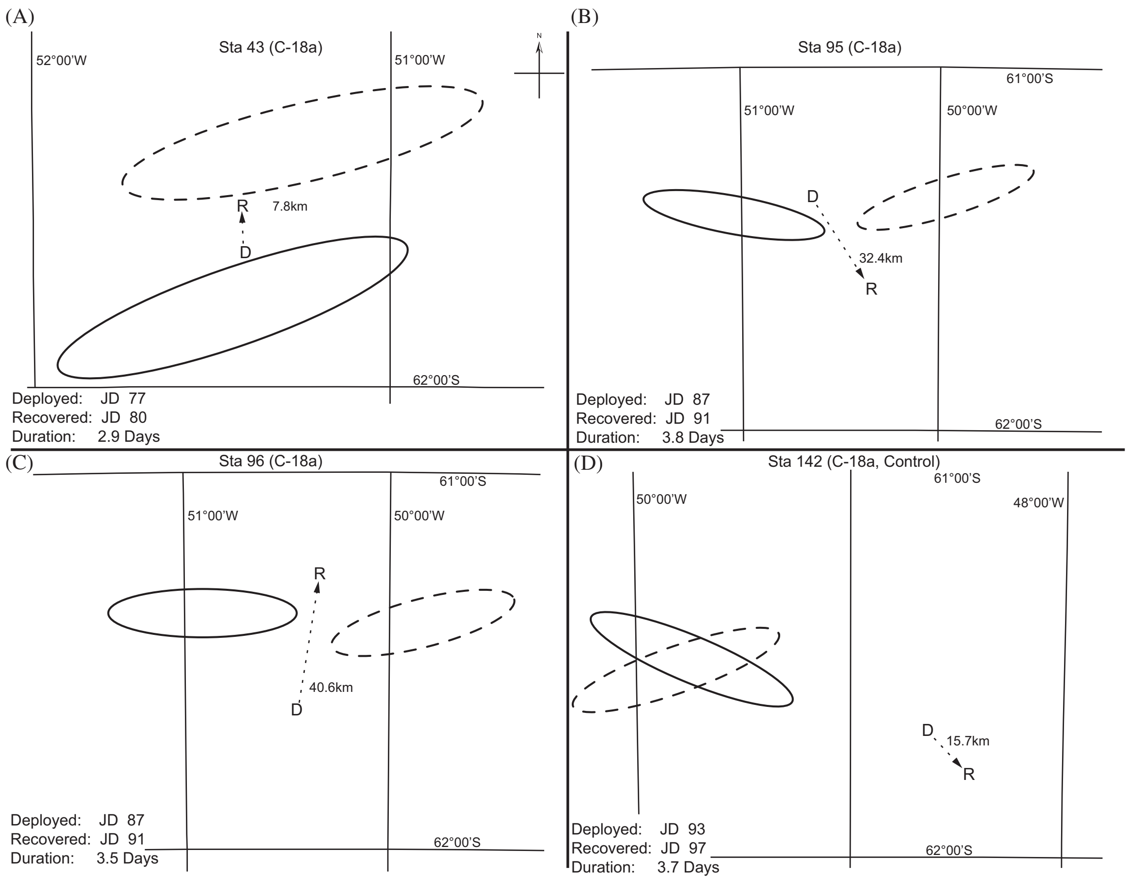

Fig. 2. Chart showing the positions of iceberg C-18a at the time of deployment (solid outline) and recovery (dotted outline) of the Lagrangian sediment traps (LST) with deployment (D) and recovery sites designated. A) LST deployment (Sta. 43) covering a distance of 7.8 km at ~500 m depth over a period of 2.9 days. B) LST deployment (Sta. 95) covering a distance of 32.4 km over a period of 3.8 days. C) LST deployment (Sta. 96) covering a distance of 40.5 km over a period of 3.5 days. D) LST deployment (Sta. 142) covering a distance of 15.7 km over a period of 3.7 days.

amorphous fecal material (Fig. 3L). Transmissivity profiles from 10 transmissometer casts concurrent with Sta. 95 and Sta. 96 revealed high variability in light transmission in the upper 200 m while reaching >98% light transmission below 200 m depth (Fig. 4). Salinity at 600 m depth ranged from 34.53 to 34.75 psu while temperature was highly variable between −0.36° to 0.41 °C.

The fourth deployment (Sta. 142) of the LST was established as a control, positioned 74 km southeast of C-18a and not in the near vicinity of other icebergs at the time of deployment (Fig. 2D). This LST drifted 15.7 km over the course of the 3.7-day deployment. Particulate matter collected during this deployment had the most diverse assemblage of diatoms of the four deployments, consisting of 12 species which were still dominated by *F. nana* and *C. pennatum* (Table 1). Many of the *C. pennatum* frustules were empty (Fig. 3M, N). Euphausiid molts were present in the samples (Fig. 3M) along with aggregated masses of phytodetritus. Fecal material consisted of a dense ovoid fecal pellet containing phytodetritus (Fig. 3O) and large numbers of string euphausiid fecal pellets (Fig. 3P). Five transmissometer profiles taken during the fourth LST deployment exhibited a sharp precipitous drop in particle density below 50 m, reaching light transmission >98% from 100 m to >600 m depth, noticeably higher than for the previous stations (Fig. 4). Salinity, 34.69 psu, and temperature, 0.47 °C, at 600 m depth were more uniform than those measured in closer proximity to C-18a.

Strong trends in size and abundance of clearly identifiable mineral grains were found between the four LST deployments. The largest and most abundant mineral grains were observed at the first station (43), with the largest grain exceeding 50 μm in two dimensions. The large grains were course and broken, showing no sign of rounding. The average grain sizes (as the product of two dimensions) at Sta. 43 were twice those observed in the following three LST deployments (Stas. 95, 96, 142). The lowest number of mineral grains were observed in the control sample from Sta 142, suggesting decreasing abundance with distance from the iceberg. Overall, the size and abundance of mineral grains are consistent with the concept that the iceberg is providing a local source of terrestrial material to the surrounding waters.

3.2. Estimates of microbial abundance and activity

Microbial abundance and activity were significantly higher in the LST samples than concurrently measured at a depth of 500 m in the same area (Table 2). The variance in values between the four LST station samples was high, but they provide a range from which to estimate the relative remineralization potential associated with sinking particulate matter in the NW Weddell Sea. Bacterioplankton cell abundance was 5 to 12 times higher in the LST samples than in seawater samples collected by a CTD/rosette at 500 m. In comparison, leucine incorporation rates were one to three orders of magnitude higher in the LST samples than in the surrounding water (Table 2). Biomass production rates were between 8 and 475 times the rates determined in 500 m water samples with generation times as short as 0.42 days at LST Sta. 95.

Algal cell abundance was two to three orders of magnitude higher in the LST samples than in the seawater samples collected at 500 m depth (Table 2). Cell abundance in the LST samples was

Table 1
Identification of the particulate matter collected in the four deployments of the LSTs around iceberg C-18a. Presence of each taxon or category in each of the four LST deployments marked with an X.

Particulate Matter	Sta. 43	Sta. 95	Sta. 96	Sta. 142
Diatoms				
Actinocyclus achtinochilus	x		x	x
Chaetoceros criophilus				x
Chaetoceros dichaeta				x
Chaetoceros sp.	x			x
Corethron pennatum	x	x	x	x
Coscinodiscus sp.	x		x	x
Fragilariopsis curta		x	x	x
Fragilariopsis nana	x	x	x	x
Fragilariopsis obliquecostata	x		x	x
Fragilariopsis pseudonana			x	
Fragilariopsis rhombica	x		x	
Fragilariopsis ritscheri		x		
Haslea sp.			x	x
Leptocylindrus mediterraneus		x		
Porosira sp.		x		
Proboscis inermis				x
Pseudonitzchia sp.			x	
Thalassiosira gracilis	x			x
Small centric diatoms (unidentified)			x	
Silicoflagellate				
Dictyocha sp.	x	x	x	x
Phytodetritus	x	x	x	x
Radiolarian	x		x	
Euphausiid exuviae (fragments, molts)	x	x		x
Fecal material				
Euphausiid string pellets (cylindrical)	x	x	x	x
Minipellets (spherical, < 50 um)	x	x	x	x
Small crustacean pellets (cylindrical, ovoid)	x	x	x	x
Salp fecal material (tabular)		x		
Larvacean fecal material (ellipsoid)		x	x	x
Fish feces (orange)	x	x		x
Fecal fluff (amorphous)	x	x	x	x
Mineral grains	x	x	x	

highest at the control station (Sta. 142), 2.45×10^5 cells ml^{-1}, and lowest at the iceberg station (Sta. 95), 1.12×10^4 cells ml^{-1}. Sinking phytoplankton particle size followed the same distribution pattern of suspended cells in the surface waters (Vernet et al., this issue), with higher sedimentation of small particles (<3 μm) and lower numbers of larger cells (>20 μm). The exception was control station (Sta. 142) where intermediate size phytoplankton cells (3-10 μm) were most abundant (Table 2).

3.3. *Flux of particulate matter:*

The mass flux estimated from each of the LST collection cups was highly variable and ranged from 589.0 mg m^{-2} d^{-1} at Sta. 96 to a low of 25.4 mg m^{-2} d^{-1} at the control station (Sta. 142; Fig. 5A). Similarly, total and organic carbon varied by an order of magnitude from highs of 12.9 and 26.2 mg C m^{-2} d^{-1}, respectively, at Sta. 96 to more consistent lows of 1.4 mg C m^{-2} d^{-1} at Sta. 43 (Fig. 5B,C). The higher organic carbon flux compared to the total carbon flux was attributable to the sampling method and having an unequal distribution of organic carbon on each half of the filter before analysis. Total nitrogen ranged from 3.7 mg N m^{-2} d^{-1} at Sta. 96 to a low of 0.2 mg N m^{-2} d^{-1} at Sta. 43 (Fig. 5D). Molar organic carbon:total nitrogen was variable between subsamples on the same deployment and between deployments, ranging from 4.25 at Sta. 43 to 11.44 at Sta. 96 (Fig. 5D).

The three stations associated with iceberg C-18a had the highest particulate fluxes, however, they exhibited the most variability in the nine subsample collections compared to the three subsamples from the control deployment (Fig. 5). We treated each flux measurement as a subsample for each of the three deployments, calculating a mean value. A collective mean flux and standard error were then determined for the particulate flux measurements from collections within 30 km of C-18a (Fig. 5). The mean mass flux (124.0±55.8 mg m^{-2} d^{-1}) and organic carbon flux (5.6±3.1 mg m^{-2} d^{-1}) are 2.7 and 2.2 times higher, respectively, than the mean subsample mass flux (45.8 mg m^{-2} d^{-1}) and organic carbon flux (2.5 mg m^{-2} d^{-1}) at the control site (Fig. 5A, C). However, due to the high variability, there was no significant difference ($p>0.05$) between the iceberg-associated mass and organic carbon fluxes and those for the control site. Similarly, the total nitrogen flux associated with C-18a (0.87±0.38 mg m^{-2} d^{-1}) was 2.3 times higher than the nitrogen flux (0.37 mg m^{-2} d^{-1}) at the control site. The difference between the iceberg associated and control stations were less apparent for total carbon, 3.9 ± 1.3 mg m^{-2} d^{-1} and 2.2 mg m^{-2} d^{-1}, respectively (Fig. 5B).

The organic C/^{234}Th activity ranged from a low of 1.6 μmoles C_{org} per DPM of ^{234}Th at Sta. 142 to a high of 4.2 μmoles C_{org} per DPM of ^{234}Th at Sta. 96. The trend in organic C_{org}/^{234}Th activity followed that of organic carbon export which is consistent with higher or more efficient organic carbon export associated with larger biogenic particles (see Shaw et al., 2011a; Buesseler et al., 2006).

The factor of two differences between the organic carbon flux data for the three C-18a LST deployments (Stas. 43, 95, 96) and the control (Sta. 142) are consistent with the ^{234}Th proxy estimates for carbon export in these locations. The flux of ^{234}Th from the upper 100 m of the water column was determined and converted to organic carbon export using organic carbon to ^{234}Th measured on LST material (see Shaw et al., 2011a). The calculated fluxes of organic carbon leaving the upper water column were about 10 times those measured in the LSTs, ranging from 36-51 mg m^{-2} d^{-1} for the C-18a stations and 23 mg m^{-2} d^{-1} at the control site (Shaw et al., 2011a). Comparison of the upper water column results with LST collections suggest that about 90% of material is regenerated during transit from 100-600 m depth.

4. Discussion

A compelling argument can be made that the mean mass and organic carbon fluxes within a radius of 30 km around iceberg C-18a (Stas. 43, 95, 96) are higher than the fluxes measured at the control site 74 km away (Sta. 142), albeit with considerable variability (Fig. 5A, C). Does the influence of C-18a extend such an extensive distance or do the collections, made over three to four days, reflect a proportionately larger sampling in closer proximity to the iceberg with lower contributions at greater distances? Previous studies have shown that free-drifting icebergs have a surrounding enrichment of chlorophyll, krill and seabirds out to a radial distance of ~3.7 km (Smith et al., 2007). It is reasonable to assume that this pelagic community enrichment contributes to particulate export fluxes that can radiate out tens of kilometers at a depth of 600 m. Neutrally buoyant sediment traps, similar to the LST, have an estimated collection range of tens of kilometers at comparable depths (Siegel et al., 2008). The surface meltwater from C-18a is detectable up to 19 km away from the iceberg and can persist for at least 10 days (Helly et al., 2011).

Assuming a collection radius of 30 km around iceberg C-18a, the influenced area would be 2826 km^2 with an estimated mass flux of 350.4 tons d^{-1} and an organic carbon export of 15.8 tons d^{-1}

(Fig. 6A). Decreasing the area of influence to 1256 km^2 (20 km radius) and 314 km^2 (10 km radius), the particulate organic carbon export estimates are 7.0 tons d^{-1} and 1.7 tons d^{-1}, respectively. Since the icebergs and the LSTs are drifting targets, representing the collection area as a circle seems reasonable and the distances from C-18a compatible with those in Fig. 5.

Extrapolation of the mass and organic carbon export fluxes around C-18a to a broader regional perspective is possible with

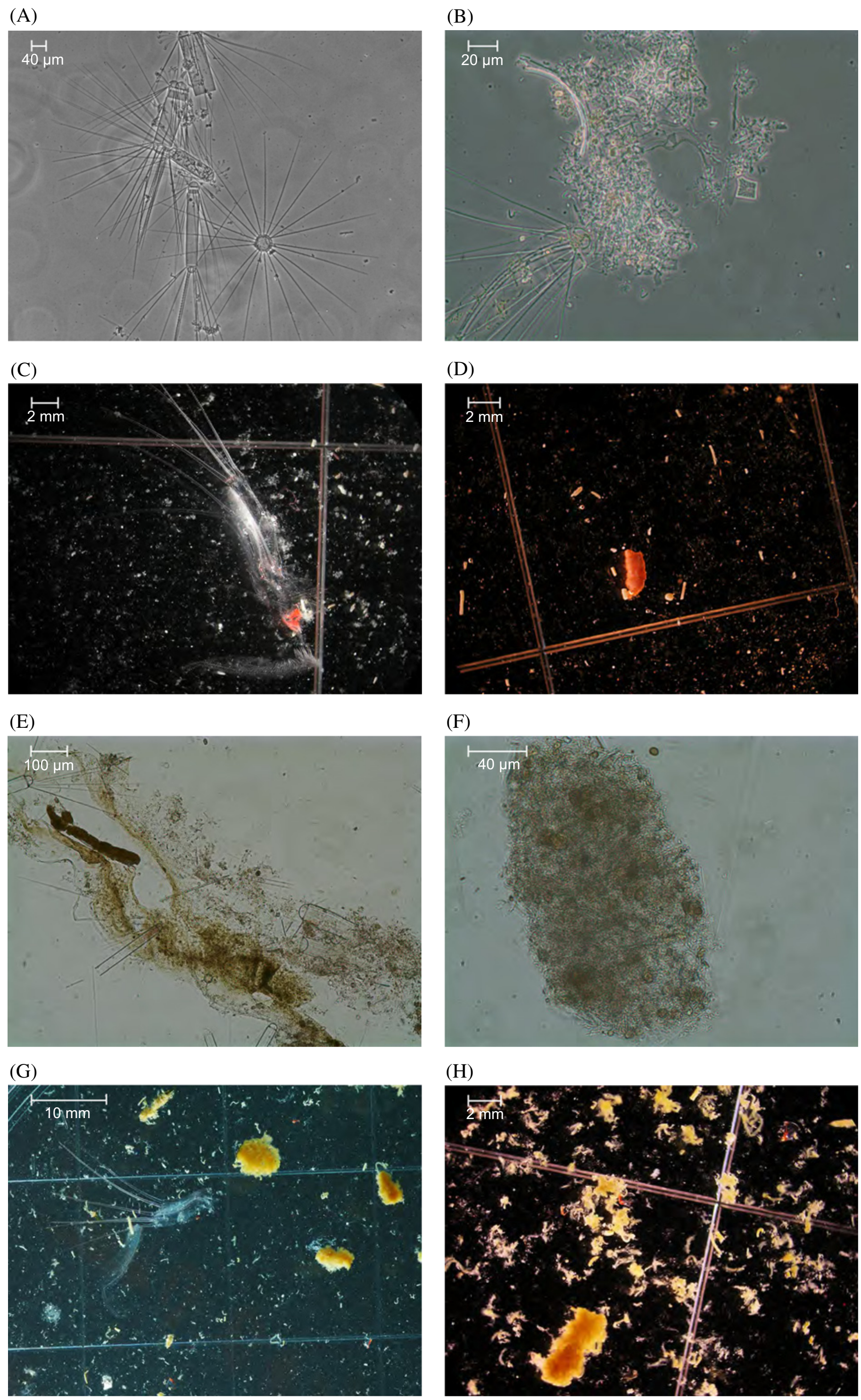

Fig. 3. Photomicrographs of particulate matter collected in the sample cups of the Lagrangian sediment traps deployed at four stations (Stas. 43, 95, 96, 142) around iceberg C-18a. A) Sta. 43; *Corethron pennatum*. B) Phytodetritus with diatom frustules of *Corethron pennatum*, *Actinocyclus achtinochilus*, *Chaetoceros* sp, and the silicoflagellate *Dictyocha speculum*. C) Fragment of a euphausiid (*Euphausia* sp.). D) Fecal material from euphausiids (brown cylindrical shape) and fish (large reddish pellet). E) Sta. 95; Phytodetritus with *C. pennatum* frustules and a euphausiid molt. F) Crustacean fecal pellet containing lipid globules and phytodetritus. G) degraded salp fecal material and euphausiid exoskeletal fragments. H) fecal fluff and large salp fecal pellet. I) Sta.96; *C. pennatum* frustules with phytodetritus. J) ruptured fecal pellet with phytodetritus. K) Cylindrical euphausiid fecal pellets and phytodetritus. L) Radiolarian "balls", amorphous phytodetritus patches and euphausiid fecal pellets. M) Sta. 142; Euphausiid molt surrounded by phytodetritus dominated by *C. pennatum* frustules. N) Phytodetritus with *C. pennatum* frustule fragments. O) Dense orange fecal pellet with diatom frustules. P) Euphausiid fecal pellets immersed in fecal fluff and phytodetritus.

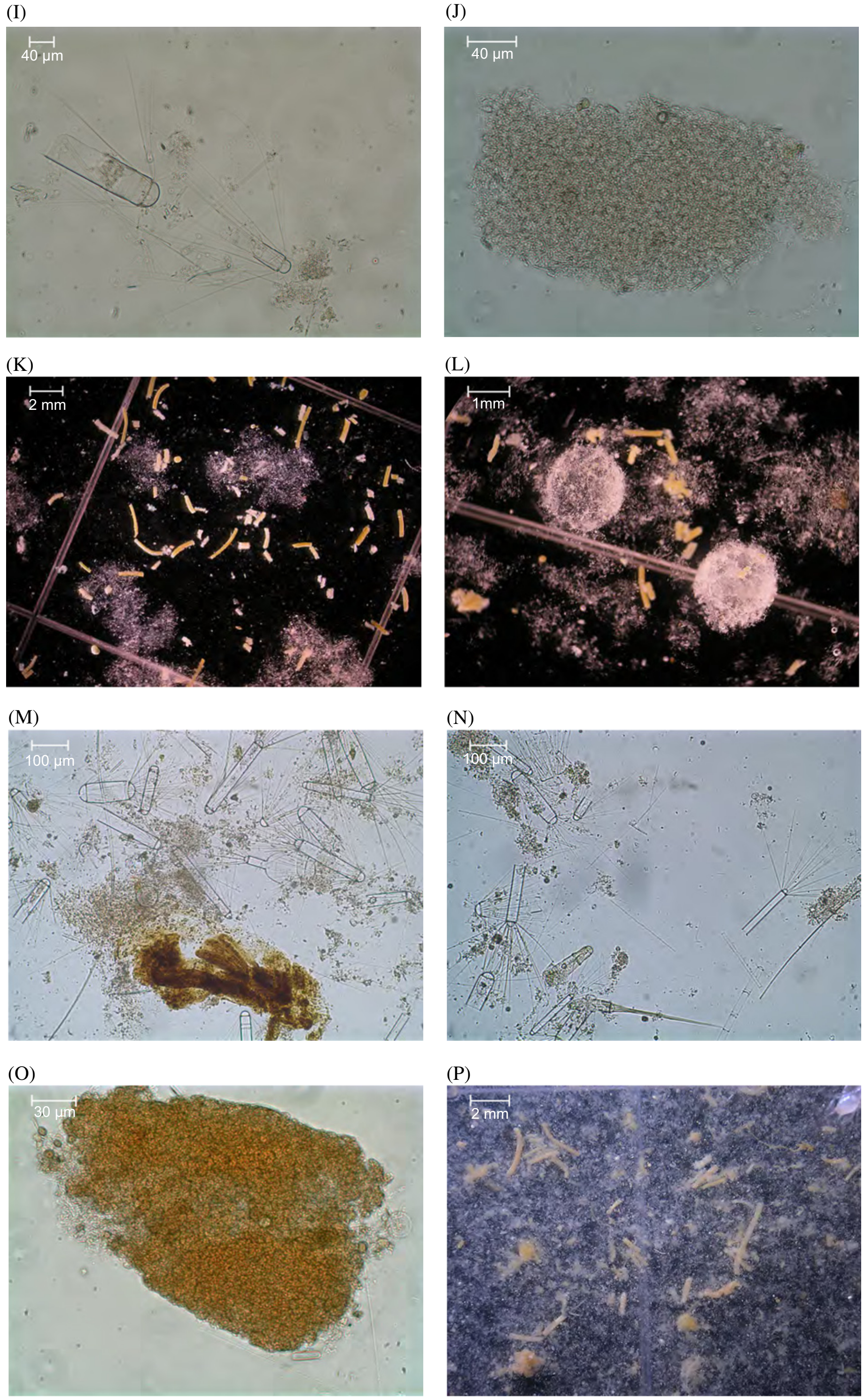

Fig. 3. (*continued*)

population estimates of similar-sized icebergs from satellite images taken over the same period of time in the Weddell Sea. Between March and April 2009, there were five icebergs of comparable size to C-18a identified in satellite images (D. Long, pers. comm.) covering an area of approximately 47,636 km^2 of the northwestern Weddell Sea (Fig. 1). The combined area of the five icebergs was 907 km^2 or 2% of the designated surface area along "Iceberg Alley". Using the estimated area of each iceberg and assuming it was circular, we calculated the area of influence with a 10, 20 and 30 km radius. Expanding the area of each iceberg by 10 km radius increased the combined area to 4752 km^2 and with a 30 km radius expanded to 21,859 km^2 or 46% of the iceberg alley area. The estimated mass flux over this extended 30-km radius area for the five icebergs was 2710.5 tons d^{-1} and the organic carbon export was 122.4 tons d^{-1} (Fig. 6B). This estimate only includes the 5 icebergs of comparable size to C-18a and not the multitude of smaller icebergs routinely

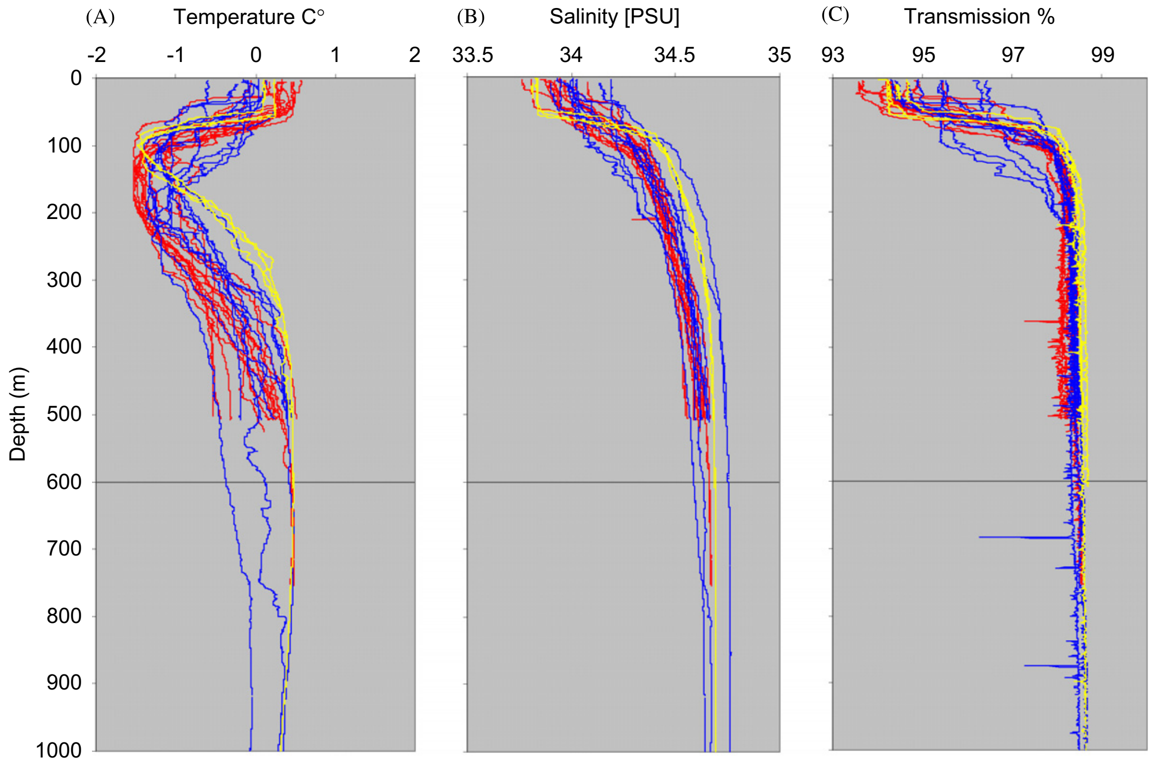

Fig. 4. Depth profiles of temperature (A), salinity (B) and percent light transmission (C) from the surface to a maximum depth of 1000 m in the vicinity and during the same time as the four LST deployments; Sta. 43 [14 casts (red)], Stas. 95 and 96 [10 casts (blue)], and Sta. 142 [5 casts (yellow)].

Table 2
Cell abundance and bacterial activity from four LST stations and from water samples taken in the near vicinity with a CTD/rosette at 500 m depth. Bacterial cell counts (both particle-associated and free-living) and protein biosynthesis rates and associated parameters were determined for three of the four LST samples. An average of six plankton samples at 500 m depth in the same region as the LST deployments was calculated as an estimate of free-living bacterioplankton. Live phytoplankton cell counts in the LST samples were estimated with flow-cytometry and divided into three different size ranges. Dead phytoplankton cells and empty diatom frustules are not included in the abundance estimates. An average concentration of phytoplankton cells from twelve CTD/rosette water samples at 500 m serves as a comparison.

Sample	Sta 43	Sta 95	Sta 96	Sta 142	500 m Plankton
Bacteria cell abundance (cells × mL^{-1})	nd	2.97×10^5	3.85×10^5	7.60×10^5	$6.51 \pm 1.31 \times 10^4$
Leucine incorporation rate (pM × hr^{-1})	36.32	167.32	2.83	42.64	0.35 ± 0.20
Bacterial biomass production (mgC × L^{-1} day^{-1})	1.31×10^{-3}	6.02×10^{-3}	0.10×10^{-3}	1.53×10^{-3}	$1.27 \pm 0.73 \times 10^{-5}$
Generation time (day)	nd	0.42	32.52	4.25	55.82 ± 27.08
Phytoplankton cell abundance (cells × mL^{-1})	2.29×10^4	1.12×10^4	2.13×10^4	2.45×10^5	$0.25+0.15 \times 10^2$
Phytoplankton >10 μm (cells × mL^{-1})	0.37×10^3	0.66×10^3	0.15×10^3	4.75×10^3	1.5+1.7
Phytoplankton 3–10 μm (cells × mL^{-1})	1.75×10^4	2.27×10^3	8.31×10^3	3.04×10^4	$0.13+0.1 \times 10^2$
Phytoplankton <3 μm (cells × mL^{-1})	5.04×10^3	8.26×10^3	1.29×10^4	2.1×10^5	$0.1+0.07 \times 10^2$

observed in the study area during the cruise. Given the increased surface area to volume ratio of smaller icebergs, their impact has been estimated to be very substantial (Smith et al., 2007).

Another important comparison is with the estimated primary production in the NW Weddell Sea. The primary production measured in the ice-edge zone in March 1986 was 126 mg C m^{-2} d^{-1} (Smith and Nelson, 1990). During our cruise in March/April 2009, primary production varied from 106.4 to 368.9 mg C m^{-2} d^{-1}, with high and variable rates in the vicinity of C-18a (Vernet et al., 2011). Using the primary production of 126 mg C m^{-2} d^{-1} as a "background rate" and extrapolating to the area encompassing the five icebergs (47,636 km^2), the estimated primary production is 6002 tons C d^{-1}. The estimated organic carbon export for the 30 km radius around the five icebergs is 122.4 tons d^{-1} at 600 m depth or 2% of the daily primary production. The percent primary production reaching depths of 500 m have been estimated to be from 1.6 to 5% in the North Pacific during summer (Buesseler et al., 2007). Again, considering the high number of smaller icebergs in the vicinity of the five larger icebergs, their contribution to export flux appears very considerable.

The sinking flux of particulate matter associated with free-drifting iceberg C-18a consisted of diatoms and heterotrophically generated fecal material. The diatom diversity was similar to that observed in surface waters (0-100 m; Cefarelli et al., 2011). *Corethron pennatum* and several species of *Chaetoceros* dominated the larger fraction of phytoplankton (>20 um). In the LST samples, *Fragilariopsis nana* and other small diatoms of the same genus also dominated numerically; their sinking could be attributed to small particle aggregation (Burd and Jackson 2009). Due to the larger size of *C. pennatum*, their contribution to the carbon flux is expected to be greater (Bienfang 1984). In the LST samples,

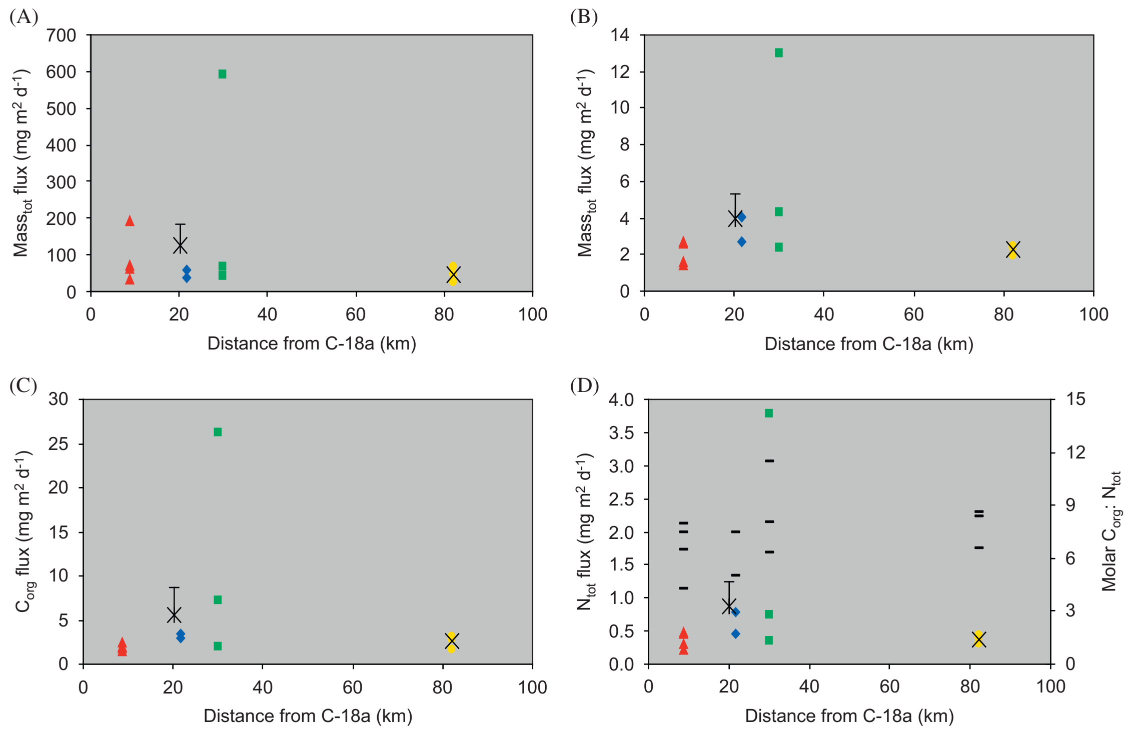

Fig. 5. Plots of mass flux (A), total carbon flux (B), organic carbon flux (c), total nitrogen flux and molar C_{org}:N_{tot} (D) with distance from iceberg C-18a. Fluxes are estimated from each subsample, collection cup, on the three deployments of the LST in the vicinity of iceberg C-18a and at the control site 74 km away. Sta. 43 (red triangle – 4 subsamples); Sta. 95 (blue diamond – 2 subsamples); Sta. 96 (green square – 3 subsamples); and Sta. 142 (yellow circle – 3 subsamples). Mean fluxes ± standard error (black crosses with whisker bars) for the three deployments in proximity to iceberg C-18a and for the one control deployment 74 km away are plotted at the mean distance from the iceberg.

most diatoms were identified from frustules and were representative of the NW Weddell Sea assemblages. These same taxa are abundant in sediments in the region (Buffen et al., 2007).

Fecal material collected in a similar area of the NW Weddell Sea between November and January 1989 was dominated by krill cylindrical strings and oval pellets in the upper 50 m, decreasing exponentially in number and dry weight with depth to 1000 m (Gonzalez, 1992). The highest abundance of fecal material was found in the Weddell-Scotia Confluence or associated with the seasonal ice edge. In areas of natural iron fertilization associated with the Kerguelan Plateau, a similar condition prevails with zooplankton grazing and the production of copepod fecal material being a primary constituent of the export flux either singly or in the abundant aggregates (Ebersbach and Trull, 2008). The export flux measured at ≤ 100 m depth in association with the iron enriched phytoplankton community around the Crozet Plateau to the northeast of the Kerguelan site was primarily diatom species with few fecal pellets (Salter et al., 2007). At these more northerly sites, the influence of krill diminishes markedly compared with areas south of the Antarctic Polar Front (Atkinson et al., 2009).

The presence of mineral grains in the LST samples validates chemical tracer evidence of significant terrestrial material delivery during iceberg transit (Smith et al., 2007; Shaw et al., 2011a). The presence of large mineral grains in LST collections in close proximity to the iceberg also indicates delivery of abundant finer grain (down to nanoscale) material to the water column. Size distribution information on ice collected during this study suggest that a minimum of 25% of the ice-borne material is less than 63 μm in size with much of that being rock flour (Shaw et al., 2011b). Similar work on glacial material suggests a significant input of nanoscale iron rich material associated with icebergs (Raiswell et al., 2006; Raiswell, 2011). Overall, these observations confirm a source for observed iron enrichments in proximity to free drifting icebergs (de Baar et al., 1995; Lin et al., 2011).

The sinking fluxes of particulate matter associated with icebergs can be compared with flux measurements made with moored and drifting sediment traps in other regions of the Southern Ocean. The most comparable particle flux measurements were conducted in the abyssal northern Weddell Sea to the east of our site (Table 3; Fig. 1). A sediment trap was moored at a depth of 863 m with sequencing collections of 11 days each during March 1985 (Fischer et al., 1988), a period not covered by seasonal pack ice and most comparable to our LST collection period. Particulate mass fluxes ranged from a high of 9.20 mg m^{-2} d^{-1} in mid-March to a low of 0.37 mg m^{-2} d^{-1} in early April, which are 1-3 orders of magnitude lower than the fluxes measured in the LST deployments (Table 3). Mass fluxes measured at 494 m depth with moored sediment traps in Bransfield Strait (Fig. 1) in March 1984 were considerably lower but the organic carbon fluxes were comparable to those measured at 600 m depth with the LSTs (Table 3).

Drifting sediment traps were deployed to measure the flux of particulate matter associated with areas of natural iron enrichment from topographic features in the S. Indian Ocean (Fig. 1). Over the Kerguelen Plateau, where local upwelling sustains higher productivity, the organic carbon fluxes measured with drifting sediment traps at 430 m depth were 3 times higher than those measured in association with iceberg C-18a (Table 3). Similarly, on the Crozet Plateau, drifting sediment traps deployed for < one day at depths of 87 and 100 m depth yielded comparable mass fluxes but order of magnitude higher organic carbon fluxes than those measured with the LSTs (Table 3). The order of magnitude difference is consistent with ^{234}Th based fluxes from

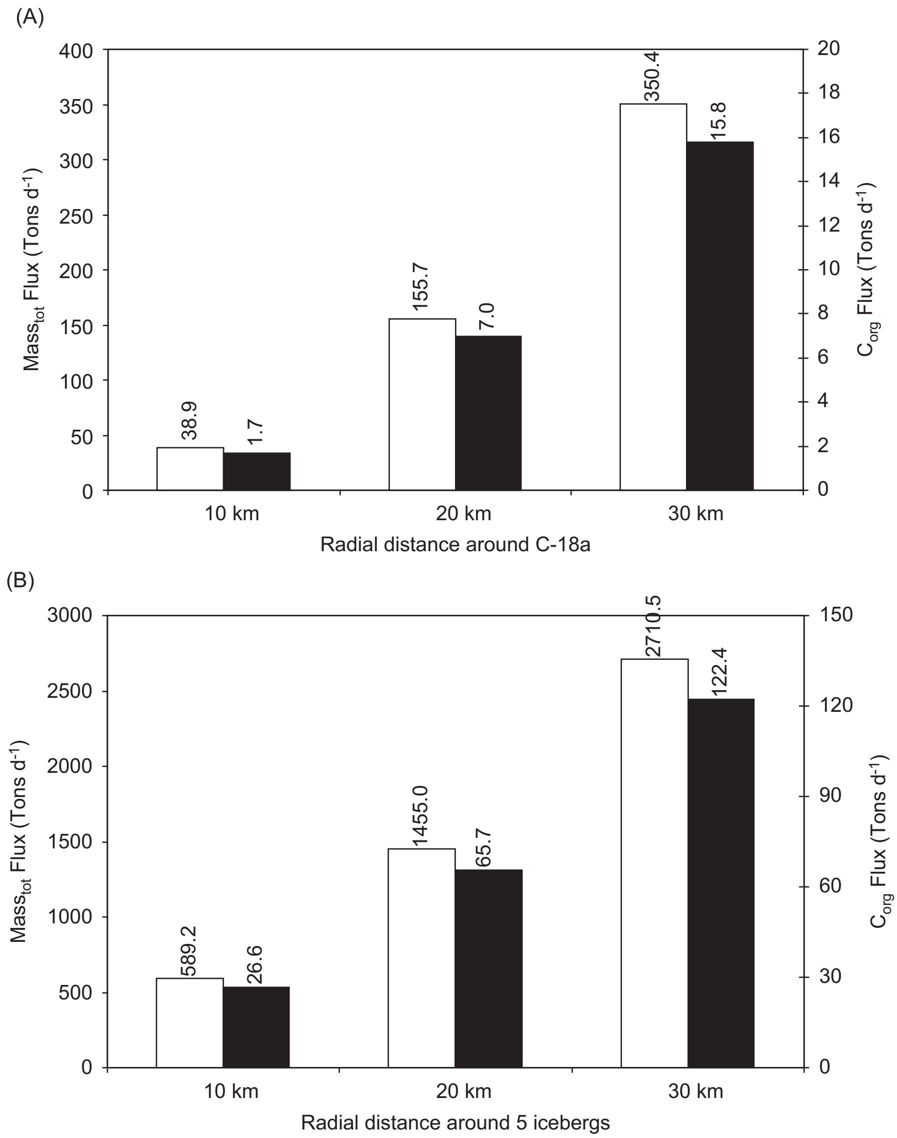

Fig. 6. Estimates of the area of circular influence around iceberg C-18a and around a broader population of five similar-sized icebergs in the same area and time within the NW Weddell Sea. (A) Area of influence expanded to 10, 20 and 30 km radius around C-18a. (B) Area of influence expanded to 10, 20 and 30 km radius around five satellite monitored icebergs.

the upper 100 meters at C-18a (Shaw et al., 2011a, 2011b). The benthic enrichment of nutrients combined with higher ambient light one to two months earlier and at lower latitude could easily account for the difference in carbon flux between the Indian Ocean sites and the C-18a site (Fig. 1).

The role of bacterial remineralization in carbon export is debated and its importance may vary from coastal to open ocean and with latitude (Baltar et al., 2009), and in anoxic basins (Taylor et al., 2009). However, it is clear that due to high microbial biomass on sinking particles (Simon et al., 2002) local remineralization rates can also be high. The proportional differences between production and export remain to be quantified for most of the ocean. Bacterioplankton abundance and biomass production based on protein synthesis rates varied significantly though are likely underestimates due to challenges in counting cells on particles (the samples were not sonicated as per Taylor et al., 2009). Additionally, low leucine incorporation rates in LST samples from Sta.96 may have been due to the lower particulate matter concentration in comparison to the other LST samples (based on visual inspection of DAPI-stained preparation) resulting in an underestimate of biomass production. POC was not determined on the same sample cup that the microbial samples were taken.

In theory, it seems plausible to measure the export of organic carbon from free-drifting icebergs of a wide range in size at different times of the year using the LSTs. However, in reality it is difficult to achieve such measurements given the logistical constraints of shiptime combined with natural constraints of Southern Ocean weather and seasonal pack ice. We feel a complementary strategy is needed in the future to measure the organic carbon export flux using moored sediment trap arrays positioned across the most frequently traveled iceberg route, ‘‘Iceberg Alley’’. Placing moored sediment traps across a hypothesized gradient from high iceberg concentrations in the northwest to lower concentrations in the central Weddell Sea at comparable depths over an entire year would provide a mechanism to estimate the export flux and sequestration of organic carbon from icebergs compared to ‘‘control’’ situations influenced by seasonal pack ice alone. These long-term studies would be done in conjunction with short-term LST deployments around a size range of icebergs. Particulate fluxes associated with individual icebergs would then

Table 3
Comparison of the total particulate mass flux and organic carbon flux measured with the LSTs with fluxes obtained in other studies using moored and drifting sediment traps at comparable depths and time of year in the Atlantic and Indian Ocean sectors of the Southern Ocean.

Location	Sampling Period[a]	Trap Type	Total Water Depth (m)	Trap Depth (m)	$Mass_{tot}$ Flux mg m^{-2} d^{-1}	C_{org} flux mg m^{-2} d^{-1}	Reference	Location
N. Weddell Sea	2/27/85–3/10/85	moored	3800	863	9.2		Fischer et al. (1988)	62° 26.5′S, 34° 45.5′W
	3/10/85–3/21/85				4.66		Fischer et al. (1988)	
	3/21/85–4/1/85				0.37		Fischer et al. (1988)	
Bransfield Strait	02/29/84–3/30/84	moored	1952	494	27.6	5	Wefer et al. (1988)	62° 15.4′S, 57° 31.7′W
	3/30/84–4/29/84				2.4	0.8*	Wefer et al. (1988)	
Drake Passage	12/2/80–1/25/81	moored	3625	965	446.6	12.7	Wefer et al. (1982); Muller et al. (1986)	60° 54.6′S, 57° 06.0′W
S. Indian Ocean	3/10/99–3/27/99	moored	4000	1400	10.6	0.47	Pilskaln et al. (2004)	62° 28.6′S, 72° 58.5′E
	3/27/99–5/6/99				12.6	0.7	Pilskaln et al. (2004)	
S. Indian Ocean, Kerguelen Plateau	2/7/05–2/8/05 A-3	drifting		430		15	Ebersbach and Trull (2008)	52° 27.43′S, 75° 36′E
	2/12/05–2/13/05		1000	430		13	Ebersbach and Trull (2008)	50° 37.7″S, 72° 00′E
S. Indian Ocean, Crozet Plateau	1/10/05	drifting	4200	87	132.9	20.6	Salter et al., (2007)	46°S, 52°E
	1/12/05			100	110.3	11.5	Salter et al., (2007)	
N.W. Weddell Sea	3/18/09–4/1/09	drifting	2918–3226	600	124	5.6	This study	61°–62°S
	4/3/09–4/7/09	drifting	3226–3277	600	45.8	2.5	This study	49°–52°W

[a] Inaccurate according to authors.

be used in combination with shipboard and satellite population estimates for comparison with concurrent broader scale export flux and sequestration measurements across "Iceberg Alley".

Our results thus far strongly suggest the importance of free-drifting icebergs on enriching the surrounding pelagic ecosystem and ultimately enhancing the export and sequestration organic carbon in the deep Southern Ocean.

Acknowledgments

This research was funded by National Science Foundation grants (ANT-0636813 to K. Smith; ANT-0636319 to T. Shaw; ANT-0636543 to A. Murray; ANT-0636730 to M. Vernet) and by the David and Lucile Packard Foundation. We thank B. Hobson and P. McGill who were instrumental in the development of the LSTs. Shipboard support was provided by B. Hobson, P. McGill, J. Ellena, and C. Hexel. Captain Watson and the crew on RVIB N.B. Palmer accompanied by the Raytheon Polar Services support group made the LST deployments and recoveries a success. J. Ellena conducted the chemical analyses and S. Wilson identified the fecal material. We thank K. Stuart and D. Long for providing the satellite data on icebergs in the vicinity of C-18a during our study and two reviewers for critical comments which greatly improved this paper.

References

Atkinson, A., Siegel, V., Pakhomov, E.A., Jessopp, M.J., Loeb, V., 2009. A re-appraisal of the total biomass and annual production of Antarctic krill. Deep-Sea Research I, 727–740.

Ballantyne, J., 2002. A multidecadal study of the number of Antarctic icebergs using scatterometer data. Brigham Young University online report: 〈http://www.scp.byu.edu/data/iceberg/IcebergReport.pdf〉.

Baltar, F., Aristegui, J., Gasol, J.M., Sintes, E., Herndl, G.,.J., 2009. Evidence of prokaryotic metabolism on suspended particulate organic matter in the dark waters of the subtropical North Atlantic. Limnology and Oceanography 54, 182–193.

de Baar, H.J.W., De Jong, J.T.M., Bakker, D.C.E., Loscher, B.M., Veth, C., Bathmann, U., Smetacek, V., 1995. Importance of iron for plankton blooms and carbon dioxide drawdown in the Southern Ocean. Nature 373, 412–415.

Bienfang, P.K., 1984. Size structure and sedimentation of biogenic microparticulates in a subarctic ecosystem. Journal of Plankton Research 6, 985–995.

Blain, S., Queguiner, B., Armand, L., Belviso, S., Bombled, B., Bopp, L., Bowie, A., Brunet, C., Brussaard, C., Carlotti, F., Christaki, U., Corbiere, A., Durand, I., Ebersbach, F., Fuda, J.-L., Garcia, N., Gerringa, L., Griffiths, B., Guigue, C., Guillerm, C., Jacquet, S., Jeandel, C., Laan, P., Lefevre, D., Monaco, C.L., Malits, A., Mosser, J., Obernosterer, I., Park, Y.-H., Picheral, M., Pondaven, P., Remenyi, T., Sandroni, V., Sarthou, G., Savoye, N., Scouarnec, L., Souhaut, M., Thuiller, D., Timmermans, K., Trull, T., Uitz, J., van Beek, P., Veldhuis, M., Vincent, D., Viollier, E., Vong, L., Wagener, T., 2007. Effect of natural iron fertilization on carbon sequestration in the Southern Ocean. Nature 446, 1070–1074.

Boyd, P., 2004. Ironing out algal issues in the Southern Ocean. Science 304, 396–397.

Boyd, P.W., Mackie, D.S., Hunter, K.A., 2009. Aerosol iron deposition to the surface ocean – Modes of iron supply and biological responses. Marine Chemistry, 2009. doi:10.1016/j.marchem.2009.01.008.

Boyd, P.W., Watson, A.J., Law, C.S., Abraham, E.R., Trull, T., Murdoch, R., Bakker, D.C.E., Bowie, A.R., Buesseler, K.O., Chang, H., Charette, M., Croot, P., Downing, K., Frew, R., Gall, M., Hadfield, M., Hall, J., Harvey, M., Jameson, G., LaRoche, J., Liddicoat, M., Ling, R., Maldonado, M.T., McKay, R.M., Nodder, S., Pickmere, S., Pridmore, R., Rintoul, S., Safi, K., Sutton, P., Strzepek, R., Tanneberger, K., Turner, S., Walte, A., Zeldis, J., 2000. Mesoscale phytoplankton bloom in the polar Southern Ocean stimulated by iron fertilization. Nature 407, 695–701.

Buesseler, K.O., Andrews, J.E., Pike, S.M., Charette, M.A., 2004. The effects of iron fertilization on carbon sequestration in the Southern Ocean. Science 304, 414–417.

Buesseler, K.O., Benitez-Nelson, C.R., Moran, S.B., Burd, A. Charette, M., Cochran, J.K., Coppola, L., Fisher, N.S., Fowler, S.W., Gardner, W.D., Guo, L.D. Gustafsson, O., Lamborg, C.,Masque, P., Miquel, J.C.,Passow, U.,Santschi, P.H., Savoye,N., Stewart, G., Trull, T., 2006. An assessment of particulate organic carbon to thorium-234 ratios in the ocean and their impact on the application of 234Th as a POC flux proxy, Marine Chemistry, FATE special issue 100, 213–233.

Buesseler, K.O., Lamborg, C.H., Boyd, P.W., Lam, P.J., Trull, T.W., Bidigare, R.R., Bishop, J.K.B., Casciotti, K.L., Dehairs, F., Elskens, M., Honda, M., Karl, D.M., Siegel, D.A., Silver, M.W., Steinberg, D.K., Valdes, J., Van Mooy, B., Wilson, S.,

2007. Revisiting carbon flux through the ocean's twilight zone. Science 316, 567–569.
Buffen, A., Leventer, A., Rubin, A., Hutchins, T., 2007. Diatom assemblages in surface sediments of the northwestern Weddell Sea, Antarctic Peninsula. Marine Micropaleontology 62, 7–30.
Burd, A.B., Jackson, G.A., 2009. Particle aggregation. Annual Review of Marine Science 1, 65–90.
Cassar, N., Bender, M.L., Barnett, B.A., Fan, S., Moxim, W.J., Levy II, H., Tilbrook, B., 2007. The Southern Ocean biological response to Aeolian iron deposition. Science 317, 1067–1070.
Cefarelli, A.O., Vernet, M., Ferrario, M.E., 2011. Phytoplankton composition and abundance in relation to free-floating Antarctic icebergs. Deep-Sea Research II 58 (11-12), 1436–1450.
Coale, K.H., Johnson, K.S., Chavez, F.P., Buesseler, K.O., Barber, R.T., Brzezinski, M.A., Cochlan, W.P., Millero, F.J., Falkowski, P.G., Bauer, J.E., Wanninkhof, R.H., Kudela, R.M., Altabet, M.A., Hales, B.E., Takahashi, T., Landry, M.R., Bidigare, R.R., Wang, X., Chase, Z., Strutton, P.G., Friederich, G.E., Gorbunov, M.Y., Lance, V.P., Hilting, A.K., Hiscock, M.R., Demarest, M., Hiscock, W.T., Sullivan, K.F., Tanner, S.J., Gordon, R.M., Hunter, C.N., Elrod, V.A., Fitzwater, S.E., Jones, J.L., Tozzi, S., Koblizek, M., Roberts, A.E., Herndon, J., Brewster, J., Ladizinsky, N., Smith, G., Cooper, D., Timothy, D., Brown, S.L., Selph, K.E., Sheridan, C.C., Twining, B.S., Johnson, Z.I., 2004. Southern Ocean iron enrichment experiment: carbon cycling in high- and low-Si waters. Science 304, 408–414.
Davis, R.E., Sherman, J.T., Dufour, J., 2001. Profiling ALACEs and other advances in autonomous subsurface floats. Journal of Atmospheric and Oceanic Technology 18, 982–993.
Dowdeswell, J., Bamber, J., 2007. Keel depths of modern Antarctic icebergs and implications for sea-floor scouring in the geological record. Marine Geology 243 (1–4), 120–131.
Ebersbach, F., Trull, T.W., 2008. Sinking particle properties from polyacrylamide gels during the Kerguelen Ocean and Plateau compared Study (KEOPS): Zooplankton control of carbon export in an area of persistent natural iron inputs in the Southern Ocean. Limnology and Oceanography 53, 212–224.
Fischer, G., Futterer, D., Gersonde, R., Honjo, S., Ostermann, D., Wefer, G., 1988. Seasonal variability of particle flux in the Weddell Sea and its relation to ice cover. Nature 335, 426–428.
Gonzalez, H.E., 1992. The distribution and abundance of krill faecal material and oval pellets in the Scotia and Weddell Seas (Antarctica) and their role in particle flux. Polar Biology 12, 81–91.
Helly, J.J., Kaufmann, R.S., Stephenson, G.R., Vernet, M., 2011. Cooling, dilution and mixing of ocean water by free-drifting icebergs in the Weddell Sea. Deep-Sea Research II 58 (11-12), 1346–1363.
Hoppema, M., 2004. Weddell Sea is a globally significant contributor to deep-sea sequestration of natural carbon dioxide. Deep-Sea Research I 51, 1169–1177.
Kirchman, D., Newell, S.Y., Hodson, R., 1986. Leucine incorporation versus biosynthesis: implications for measuring rates of protein synthesis and biomass production by bacteria in marine systems. Marine Ecology Progress Series 32, 47–59.
Lam, P.J., Bishop, J.K.B., 2007. High biomass, low export regimes in the Southern Ocean. Deep-Sea Research II 54, 601–638.
Le Quere, C., Rodenbeck, C., Buitenhuis, E.T., Conway, T.J., Langenfelds, R., Gomez, A., Labuschagne, C., Ramonet, M., Nakazawa, T., Metzl, N., Gillett, N., Heimann, M., 2007. Saturation of the Southern Ocean CO_2 sink due to recent climate change. Science 316, 1735–1738.
Lin, H., Rauschenberg, C., Hexel, C.R., Shaw, T.J., Twining, B.S., 2011. Free-drifting icebergs as sources of iron to the Weddell Sea. Deep-Sea Research II 58 (11-12), 1392–1406.
Muller, P.J., Suess, E., Ungerer, C.A., 1986. Amino acids and amino sugars of surface particulate and sediment trap material from waters of the Scotia Sea. Deep-Sea Research A 33, 819–838.
Pilskaln, C.H., Manganini, S.J., Trull, T.W., Armand, L., Howard, W., Asper, V.L., Massom, R., 2004. Geochemical particle fluxes in the southern Indian Ocean seasonal ice zone: Prydz Bay region, East Antarctica. Deep-Sea Research I 51, 307–332.
Pollard, R.T., Salter, I., Sanders, R.J., Lucas, M.I., Moore, C.M., Mills, R.A., Stratham, P.J., Allen, J.T., Baker, A.R., Bakker, D.C.E., Charette, M.A., Fielding, S., Fones, G.R., French, M., Hickman, A.E., Holland, R.J., Hughes, A., Jickells, T.D., Lampitt, R.S., Morris, P.J., Nedelec, F.H., Nielsdottir, M., Planquette, H., Popova, E.E., Poulton, A.J., Read, J.F., Seeyave, S., Smith, T., Stinchcombe, M., Taylor, S., Thomalla, S., Venables, H.J., Williamson, R., Zubkov, M.V., 2009. Southern Ocean deep-water carbon export enhanced by natural iron fertilization. Nature 457, 577–581.
Porter, K.G., Feig, Y.S., 1980. The use of DAPI for identifying and counting aquatic microflora. Limnology and Oceanography 25, 943–948.
Raiswell, R.W., 2011. Iceberg-hosted nanoparticulate Fe in the Southern Ocean: mineralogy, origin, dissolution kinetics and source of bioavailable Fe. Deep-Sea Research II 58 (11-12), 1364–1375.
Raiswell, R.W., Tranter, M., Benning, L.G., Siegert, M., De'ath, R., Huybrechts, P., Payne, T., 2006. Contributions from glacially derived sediment to the global iron oxyhydroxide cycle: implications for iron delivery to the oceans. Geochemica et Cosmochimica Acta 70, 2765–2780.
Salter, I., Lampitt, R.S., Sanders, R., Poulton, A., Kemp, A.E.S., Boorman, B., Saw, K., Pearce, R., 2007. Estimating carbon, silica and diatom export from a naturally fertilized phytoplankton bloom in the Southern Ocean using PELAGRA: a novel drifting sediment trap. Deep-Sea Research II, 2233–2259.
Shaw, T.J., Smith Jr., K.L., Sherman, A.D., Hexel, C.R., Dudgeon, R., Vernet, M., Kaufmann, R.S., 2011a. ^{234}Th-based carbon export around free-drifting icebergs in the Southern Ocean. Deep-Sea Research II 58 (11-12), 1384–1391.
Shaw, T.J., Raiswell, R.W., Hexel, C.R., Vu, H.P., Moore, W.S., Dudgeon, R., Smith Jr., K.L., 2011b. Input, composition and potential impact of terrigenous material from free-drifting icebergs in the Weddell Sea. Deep-Sea Research II 58 (11-12), 1376–1383.
Sherlock, R.E., Reisenbichler, K.R., Bush, S.L., Osborn, K.J., Robison, B.R., 2011. Near-field zooplankton, ice-face biota, and proximal hydrography of free-drifting Antarctic icebergs. Deep-Sea Research II 58 (11-12), 1457–1468.
Sherman, A.D., Hobson, B.W., McGill, P.R., Davis, R., Smith Jr., K.L., 2011. Lagrangian sediment traps for sampling at discrete depths beneath free-drifting icebergs. Deep-Sea Research II 58 (11-12), 1327–1335.
Siegel, D.A., Fields, E., Buesseler, K.O., 2008. A bottom-up view of the biological pump: modeling source funnels above ocean sediment traps. Deep-Sea Research I 55, 108–127.
Simon, M., Grossart, H.-P., Schweitzer, B., Ploug, H., 2002. Microbial ecology of organic aggregates in aquatic ecosystems. Aquat. Microb. Ecol. 28, 175–211.
Smith, D.C., Azam, F., 1992. A simple, economical method for measuring bacterial protein synthesis rates in seawater using 3H-leucine. Marine Microbial Foodwebs 6, 107–114.
Smith Jr., K.L., 2011. Free-drifting icebergs in the Southern Ocean; an overview. Deep-Sea Research II 58 (11), 1277–1284.
Smith Jr., K.L., Robison, B.H., Helly, J.J., Kaufmann, R.S., Ruhl, H.A., Shaw, T.J., Twining, B.S., Vernet, M., 2007. Free-drifting icebergs: hot spots of chemical and biological enrichment in the Weddell Sea. Science 317, 478–482.
Smith Jr., W.O., Nelson, D.M., 1990. Phytoplankton growth and new production in the Weddell Sea marginal ice zone in the austral spring and autumn. Limnology and Oceanography 35, 809–821.
Stuart, K.M., Long, D.G., 2011. Tracking large tabular icebergs using the SeaWinds Ku-band microwave scatterometer. Deep-Sea Research II 58 (11-12), 1285–1300.
Taylor, G.T., Thunell, R., Varela, R., Benitez-Nelson, C., Scranton, M.I., 2009. Hydrolytic ectoenzyme activity associated with suspended and sinking organic particles within the anoxic Cariaco Basin. Deep-Sea Research II 56, 1266–1283.
Vernet, M., Sines, K., Chakos, D., Cefarelli, A., Ekern, L., 2011. Impacts on phytoplankton dynamics by free-drifting icebergs in the NW Weddell Sea. Deep-Sea Research II 58 (11-12), 1422–1435.
Wefer, G., Fischer, G., Fuetterer, D., Gersonde, R., 1988. Seasonal particle flux in the Bransfield Strait, Antarctica. Deep-Sea Research A 35, 891–898.
Wefer, G., Suess, E., Balzer, W., Liebezeit, G., Muller, P.J., Ungerer, C.A., Zenk, W., 1982. Fluxes of biogenic components from sediment trap deployment in circumpolar waters of the Drake Passage. Nature 299, 145–147.